Testing Uncertainty Estimation and Validation Procedures in the Flow Around a Backward Facing Step

Luís Eça and Martin Hoekstra

Abstract

This paper presents an evaluation of a method for the estimation of the discretization uncertainty based on a Least Squares version of the Grid Convergence Index and a recently proposed Validation procedure in the calculation of the two-dimensional flow of an incompressible fluid over a backward facing step. Solution Verification studies are performed for three grid sets with the finite-difference and finite-volume versions of PARNASSOS using the one-equation turbulence model of Spalart & Allmaras model and the baseline and shear-stress transport variants of the $k-\omega$ two-equation turbulence models, proposed by Menter. The results show that it is difficult to obtain reliable estimates of the uncertainty of flow quantities in turbulent flows. With a procedure based on the determination of the observed order of accuracy, the level of grid refinement and/or solution accuracy required to obtain reliable estimates of the numerical uncertainty is much finer than what is commonly used nowadays. The proposed procedure for Validation is clearly more reliable than the popular graphical comparison of predictions and experiments.

1 Introduction

The significant increase of the use of Computational Fluid Dynamics in engineering applications leads inevitably to a need to establish the credibility of the numerical results. This goal may be achieved with Verification and Validation, which comprise three different stages, [1]:

1. Code Verification.
2. Solution/Calculation Verification.
3. Validation.

The first two activities are purely mathematical, whereas the third is a science/engineering activity that intends to assess the suitability of the mathematical model as a representation of the physical problem. The 3rd Workshop on CFD uncertainty analysis [2] deals with all three stages, using manufactured solutions [3, 4] for Code Verification and the flow over a backward facing step for Solution Verification and Validation.

Code Verification has been extensively performed in [4, 5, 7, 8] for the finite-difference [9] and finite-volume [10] 2-D versions of the PARNASSOS flow solver. Therefore, in this paper we focus on Solution Verification and Validation, using the same solvers.

An updated version of the discretization uncertainty estimation procedure presented in [8] is tested in three grid sets for the Spalart & Allmaras model [11] and two grid sets for the baseline (BSL) and shear-stress transport (SST) versions of the $k-\omega$ model [12], originally proposed by Wilcox in [13]. The sets range from unreasonably coarse grids (41×41) to grids which are much finer than those used

for the second edition of the Workshop [8]. The aim is to check the performance of the uncertainty estimation procedure for grids clearly outside the asymptotic range by studying the consistency of the estimated error bars at different grid levels.

In the finite-difference version of the code, we test first and third-order discretizations of the convective terms of the turbulence quantities transport equations. Thus the impact of the common choice of first-order convection in the turbulence models (to prevent nominally positive-definite quantities from becoming negative) on the accuracy of the solutions. Moreover, it also provides an extra check for the discretization uncertainty estimation procedure by having solutions of different formal accuracy in the same grids.

The forthcoming Validation Procedure proposed by the ASME V&V 20 Committee [14] will be tried in a simplified form, i.e. with the strong model concept (parameter uncertainty equal to 0) [15].

The paper is organized in the following way: section 2 gives the description of the updated version of the procedure to estimate the discretization uncertainty; the main properties of the two versions of the PARNASSOS flow solver are summarized in section 3; the Solution Verification exercise is presented in section 4 and the Validation exercise in section 5; finally, the main conclusions of this study are summarized in section 6.

2 Discretization uncertainty estimation

The basis for the estimation of the discretization uncertainty U of the solution of an integral or local flow quantity on a given grid is the standard Grid Convergence Index (GCI) method [1], which says

$$U = F_s|\delta_{RE}| \,. \tag{1}$$

F_s is a safety factor and δ_{RE} is the error estimator.

The error estimation is preferably obtained by Richardson extrapolation:

$$\delta_{RE} = \phi_i - \phi_o = \alpha h_i^p \,, \tag{2}$$

where ϕ_i is the numerical solution of any local or integral scalar quantity on a given grid (designated by the subscript $_i$), ϕ_o is the estimated exact solution, α is a constant, h_i is a parameter which identifies the representative grid cell size and p is the observed order of accuracy.

If results on more than three grids are available, ϕ_o, α and p are obtained with a least squares root approach that minimizes the function:

$$S(\phi_o, \alpha, p) = \sqrt{\sum_{i=1}^{n_g} \left(\phi_i - (\phi_o + \alpha h_i^p)\right)^2} \,, \tag{3}$$

where n_g is the number of grids available[1]. The minimum of $S(\phi_o, \alpha, p)$ is found by setting its derivatives with respect to ϕ_o, p_j and α_j equal to zero, [16]. The standard deviation of the fit[2],

[1] If $n_g = 3$, the solution of (3) is equivalent to the solution of (2). Therefore, at least four geometrically similar grids must be available to have a least squares root solution.

[2] Obviously, the standard deviation of the fit is zero for $n_g = 3$.

U_s, is given by

$$U_s = \sqrt{\frac{\sum_{i=1}^{n_g} \left(\phi_i - (\phi_o + \alpha h_i^p)\right)^2}{n_g - 3}} \,. \tag{4}$$

The ability to estimate the error with Richardson extrapolation depends on the apparent convergence condition, being one of the following options:

- Monotonic convergence.
- Oscillatory convergence.
- Monotonic divergence.
- Oscillatory divergence.

Having a single grid triplet with $h_2/h_1 = h_3/h_2$, it is not difficult[3] to classify the apparent convergence condition from the convergence ratio:

$$R = \frac{\phi_2 - \phi_1}{\phi_3 - \phi_2} \,,$$

where ϕ_1 stands for the finest grid solution, ϕ_2 for the medium grid and ϕ_3 for the coarsest grid solution. As mentioned by Roache, [17], we have:

$$\begin{aligned} 0 < R < 1 &\quad\Rightarrow\quad \text{Monotonic convergence} \\ -1 < R < 0 &\quad\Rightarrow\quad \text{Oscillatory convergence} \\ R > 1 &\quad\Rightarrow\quad \text{Monotonic divergence} \\ R < -1 &\quad\Rightarrow\quad \text{Oscillatory divergence} \end{aligned}$$

When more than three grids are available and the least squares root approach is followed, this classification is not as straightforward, because the data may exhibit scatter, [16]. First, we establish the apparent order of convergence p from the least squares solution of equation (3). Next, oscillatory convergence or divergence is identified by n_{ch}, the number of times the difference between consecutive solutions changes sign, i.e. $\left(\phi_{i+1} - \phi_i\right) \times \left(\phi_i - \phi_{i-1}\right) < 0$. The apparent convergence condition is then decided as follows:

1. $p > 0$ for $\phi \Rightarrow$ Monotonic convergence.
2. $p < 0$ for $\phi \Rightarrow$ Monotonic divergence.
3. $n_{ch} \geq INT(n_g/3) \Rightarrow$ Oscillatory convergence or divergence.
4. Otherwise $\Rightarrow$ Unknown.

[3] This does not mean that the classification based on a grid triplet is reliable.

The present way of determining oscillatory behaviour does not distinguish convergence from divergence. Furthermore, the apparent convergence condition may be unknown if the first three criteria listed above are not met. In principle, if the code has been verified, i.e. shown to be free of bugs in the implementation of the numerical model, one would not expect non-convergent situations to occur. However, for data outside the asymptotic range it is possible that apparent divergence conditions are obtained as a consequence of too coarse grids. Therefore, only three conditions are relevant for our estimation procedure:

1. Monotonic convergence.
2. Oscillatory behaviour.
3. Anomalous behaviour.

The only condition which allows an error estimation based on Richardson extrapolation is monotonic convergence. But even then small perturbations in the data may lead to significant changes in the estimated value of p, and thus to sometimes unsatsfactory results when the G.C.I. in the least-squares sense is applied.

In an attempt to overcome this, we have prevously chosen the maximum difference between all the solutions available, Δ_M,

$$\Delta_M = \max\left(|\phi_i - \phi_j|\right) \text{ with } 1 \leq i \leq n_g \wedge 1 \leq j \leq n_g \,. \tag{5}$$

as an additional parameter in the procedure. Now we introduce two others, viz. error estimators based on power series expansions with fixed exponents:

$$\delta_{RE}^{12} = \phi_i - \phi_o = \alpha_1 h_i + \alpha_2 h_i^2 \tag{6}$$

and

$$\delta_{RE}^{02} = \phi_i - \phi_o = \lambda_1 h_i^2 \,. \tag{7}$$

δ_{RE}^{12} and δ_{RE}^{02} are also calculated in the least squares sense and so we will have standard deviations given by

$$U_s^{12} = \sqrt{\frac{\sum_{i=1}^{n_g}\left(\phi_i - (\phi_o + \alpha_1 h_i + \alpha_2 h_i^2)\right)^2}{n_g - 3}} \tag{8}$$

and

$$U_s^{02} = \sqrt{\frac{\sum_{i=1}^{n_g}\left(\phi_i - (\phi_o + \lambda_1 h_i^2)\right)^2}{n_g - 3}} \tag{9}$$

We can summarize our procedure for the estimation of the numerical uncertainty, valid for a nominally second-order accurate method, as follows:

1. The observed order of accuracy is estimated with the least squares root technique to identify the apparent convergence condition according to the definition given above.

2. For monotonic convergence:

   - For $0.95 \leq p < 2.05$

$$U_\phi = 1.25\left(\delta_{RE} + U_s\right) .$$

   - For $0 < p < 0.95$

$$U_\phi = \min\left(1.25\left(\delta_{RE} + U_s\right), 1.25\min\left(1.6, 2.28/p - 1.4\right)\left(\delta_{RE}^{12} + U_s^{12}\right)\right) .$$

   - For $p \geq 2.05$

$$U_\phi = \max\left(1.25\left(\delta_{RE} + U_s\right), 1.25\min\left(1.6, 3p - 5.15\right)\left(\delta_{RE}^{02} + U_s^{02}\right)\right) .$$

3. For oscillatory convergence :

$$U_\phi = 3\Delta_M .$$

4. In other conditions:

$$U_\phi = \min\left(3\Delta_M, 3\left(\delta_{RE}^{12} + U_s^{12}\right)\right) .$$

The change in the safety factor for $p < 0.95$ and $p > 2.05$ reflects the decrease of confidence in the extrapolation. Obviously, the limits are chosen in an ad-hoc way (numerical experimentation in a limited number of cases). At present, we have selected a continuous linear change of the safety factor with a maximum value of 2 for $p \leq 0.76$ or $p \geq 2.25$.

The apparent divergence condition is included in the "anomalous behaviour" category, which may be questionable. In smooth flow fields, such apparent condition should only appear in data clearly outside the asymptotic range. However, our previous experience has shown that in cases where the scatter is similar to changes between grids we can obtain a misleading classification of "apparent divergence". Obviously, we have no guarantee that the approach is conservative for the case of data clearly outside the asymptotic range.

3 PARNASSOS flow solver

The 2-D versions of PARNASSOS solve the steady, incompressible, Reynolds-averaged Navier Stokes equations using eddy-viscosity turbulence models. Details of the implementation of the two versions are given in [9] and [10]. The main properties of the two versions are summarized below.

- The finite-difference, FD, version discretizes the continuity and momentum equations written in Contravariant form, which is a weak conservation form. The finite-volume, FV, version discretizes the strong conservation form of the equations.

- The FD version computes the momentum balance along the directions of the curvilinear coordinate system, whereas the FV version calculates the momentum balance for its Cartesian components.
- The FD code has a fully-collocated arrangement with the unknowns and the discretization centered at the grid nodes. In the FV code unknowns are defined at cell centres.
- Both versions apply quasi-Newton linearization to the convective terms and are at least second order accurate for all the terms of the continuity and momentum equations. Third-order upwind discretisation is applied to the convective terms.
- The linear system of equations formed by the discretized continuity and momentum equations is in both versions solved simultaneously, using GMRES, [18], with a coupled ILU preconditioning.
- Under-relaxation is applied with a quasi time-derivative term.
- The transport equations for the turbulence quantities are discretized with first or third-order (with our without limiters) upwind schemes.
- The linearization procedure of the production and dissipation terms of the turbulence quantities follows the standard approach, i.e. production is added to the right-hand side and dissipation to the main-diagonal.
- The solution of the turbulence quantities transport equations is uncoupled from solving the continuity and momentum equations.

4 Solution Verification

4.1 Computational domain, flow and boundary conditions

The computational domain of the flow around a backward facing step is bounded by two walls and two x constant planes, $-4H$ upstream and $40H$ downstream of the step, where H is the step height. The Reynolds number based on the step height and the velocity of the incoming flow, U_{ref}, is 5×10^5.

In the present calculations, we have specified all the required flow quantities at the inlet, with the exception of the pressure coefficient, using the profiles generated for the Workshop [19]. The pressure coefficient is extrapolated from the interior of the domain, assuming that its second derivative in the streamwise direction is zero.

At the walls, the no-slip and impermeability conditions are applied, which leads to $u_x = u_y = 0$. $\tilde{\nu}$ and k are set equal to 0 and ω is specified at the first two nodes away from the wall using the near wall solution of the ω transport equation given in [13].

In the finite-difference version of the method, the momentum equation in the normal direction is solved at the wall to obtain the pressure value; in the finite volume version the pressure at the wall is found from linear extrapolation from the interior of the domain. At the outlet boundary, u_x, u_y and the turbulence quantities are linearly extrapolated from the interior of the domain. The pressure coefficient is set to zero.

4.2 Calculation details

All the calculations were performed with 15-digits precision and the iterative error was reduced to machine accuracy. In such conditions, it is logic to assume that the contributions of the round-off and iterative errors to the numerical uncertainty is negligible compared to the discretization error.

4.3 Grid sets

We have selected two sets of 19 single-block, structured, geometrically similar grids, A and B, to perform the calculations of the flow over a backward facing step with the finite-difference version of PARNASSOS. The finite-volume version was used in a third set of 16 systematically refined grids, designated by FV.

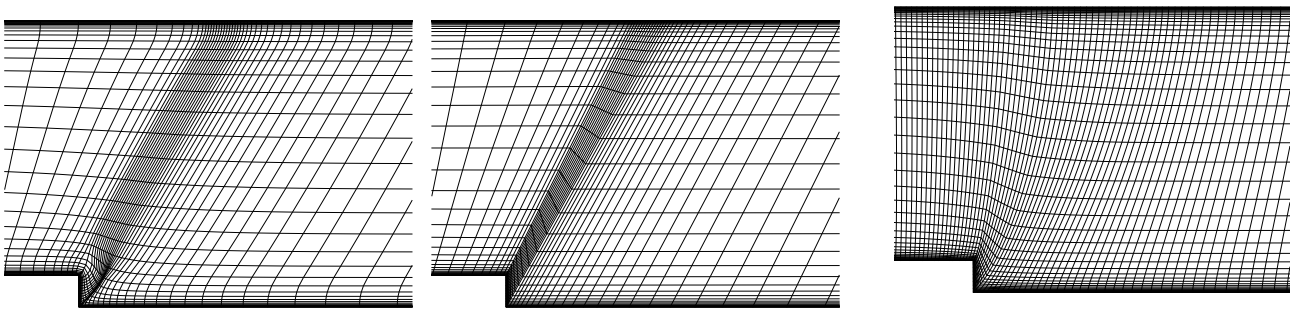

Figure 1: Illustration of the three grids sets for the calculation of the flow over a backward facing step.

- Set A is similar to the first grid set proposed for the first edition of the Workshop, [19], containing non-orthogonal curvilinear grids with the same number of nodes in both directions. At the walls the grids are orthogonal.

- Set B is the same as the set B used in the first edition of the Workshop, [19], and has straight lines connecting the bottom and top walls and the same number of nodes in both directions.

- FV includes non-orthogonal curvilinear grids with the number of nodes in the streamwise direction equal to twice the number of nodes in the normal direction. Unlike sets A and B, the set FV has the unfavourable feature that the lower (concave) corner of the step does not coincide with a grid node in all grids.

Sets A and B have coarsest grids of 41×41 nodes and finest grids of 401×401 nodes covering a grid refinement ratio of 10. For FV, the coarsest grid has 161×81 nodes and the finest 801×401 nodes. The grids in the vicinity of the step are illustrated in figure 1.

4.4 Testing the discretization estimation procedure

One of the aims of the present study is to test the reliability of the uncertainty estimation procedure even in grids clearly outside the asymptotic range. To this end, we have performed 10 grid refinement studies with the finite-difference version and the following turbulence models:

- Spalart & Allmaras model [11]:
  - Sets A and B with first and third-order discretizations of the convective terms of the $\tilde{\nu}$ transport equation.
- BSL $k-\omega$ model [12]:
  - Sets A and B with first and third-order discretizations of the convective terms of the k and ω transport equations.
- SST $k-\omega$ model [12]:
  - Sets A and B with third-order discretizations of the convective terms of the k and ω transport equations.

In both grid sets, there are 19×19 grid node locations common to all members of the set, therefore requiring no interpolation to evaluate the convergence properties with the grid refinement. Naturally, these locations are not identical in both sets. So for set B we have used local bi-cubic interpolation to obtain the solution at the fixed locations from set A.

For the two Cartesian velocity components, u_x and u_y, and pressure coefficient[4], C_p^*, we have computed the following quantities:

- Percentage of locations with estimated discretization uncertainty greater than 10^{-4} for u_x and 10^{-5} for u_y and C_p^*, N_ϕ.
- For the N_ϕ locations:
  - The percentage of locations with apparent monotonic convergence, Nc_ϕ.
  - For the Nc_ϕ locations:
    - The mean apparent order of convergence, p_{med}.
    - The minimum apparent order of convergence, p_{min}.
    - The maximum apparent order of convergence, p_{max}.
    - The percentage of locations in four different ranges of p: $p<0.095$, $0.95\le p<2.05$, $2.05\le p<3.05$, $p>3.05$.

These parameters were estimated for three different levels of grid refinement:

1. 401×401 grid using the data of the 11 finest grids covering a grid refinement ratio of 2, designated by Level 1.

[4] $C_p^* = (p-p_{outlet})/(\rho U_{ref}^2) = 1/2C_p$

2. 201×201 grid using the data of 6 grids covering a grid refinement ratio of 2, designated by Level 2.

3. 101×101 grid using the data of the 4 coarsest grids covering a grid refinement ratio of 2.5, designated by Level 3.

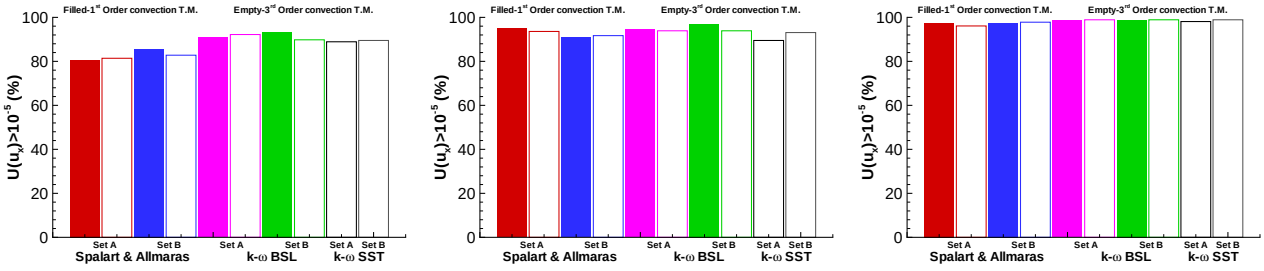

Level 1 **Level 2** **Level 3**

Figure 2: Percentage of locations with estimated discretization uncertainty of the horizontal velocity component above 10^{-4}. Calculation of the flow over a backward facing step.

Figure 2 presents N_{u_x} for the three levels tested. Expectedly, N_{u_x} increases with the grid coarsening. However, the minimum value obtained for the Level 1 is still above 80%. Similar results are obtained for u_y and C_p.

The percentage of locations of apparent monotonic convergence is illustrated in figure 3 for the three mean flow variables. The results are somehow unexpected. There is no clear trend indicating a reduction of N_c with the coarsening of the grids and in some cases the tendency seems to be exactly the opposite. Furthermore, from the different options included in the data, only the kind of flow quantity seems to have a minor influence on the trends observed in N_c. Different grid sets, turbulence models and discretizations of convection in the turbulence models lead to changes in N_c with the coarsening of the grid selected for the uncertainty estimation.

The mean value of the estimated order of convergence, p_{med}, at the locations with apparent monotonic convergence is plotted in figure 4. The data confirm the difficulties in the estimation of p in turbulent flow calculations. We should expect an increase of p_{med} with the change from first to third-order in the turbulence models convection, but that is not always the case. p_{med} should be closer to 2 for the finest grids, but there are cases where the difference to 2 is actually decreasing with the coarsening of the grid. The only expected trend observed is that p_{med} depends on the selected turbulence model.

The minimum values of p are systematically too close to 0 (around 0.1) and the maximum values of p are always above 5 and in most of the cases 6. In order to give a clear illustration of the difficulties in the p estimation, figure 5 presents the distribution of p for u_x at the three levels for the discretization uncertainty estimation.

With very few exceptions, the percentage of locations with p in the expected range ($0.95 \leq p < 2.05$) is always smaller than 50% and in some cases it is close to 20%. There is no tendency of increase of this percentage with grid refinement. In fact, there are four cases with the largest percentage of grid nodes in the expected range for the coarsest grids (level 3)! With very few exceptions, the percentage of locations with $p > 3.05$ is marginal, but the percentages for the $p < 0.95$ and $2.05 \leq p < 3.05$ ranges depend on the turbulence model. The lowest range of p is most frequent for the $k-\omega$ models, whereas for the Spalart & Allmaras model the other range is dominant.

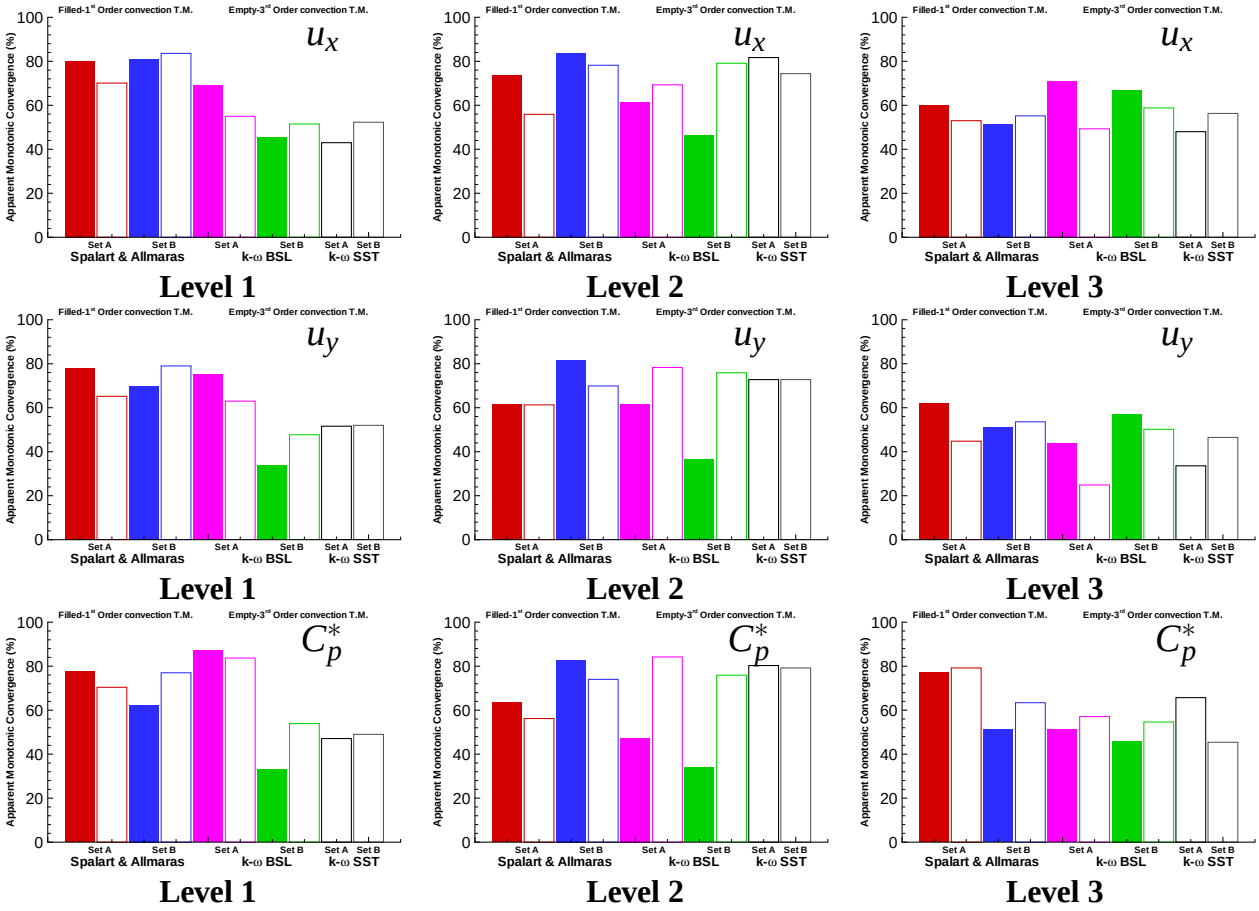

Figure 3: Percentage of locations with apparent monotonic convergence. Calculation of the flow over a backward facing step.

The evaluation of the performance of the proposed procedure for the estimation of the discretization uncertainty is made checking the overlap of the different error bars obtained. The first (and simplest) check is performed for the same grid refinement study, i.e. for a given grid refinement study, we have computed the number of locations where the error bars from levels 1, 2 and 3 do not overlap. The results are plotted in figure 6.

Bearing in mind the grid refinement of the grids included in level 3 (101×101 to 41×41), the results are not discouraging. Furthermore, if we repeat the same exercise only for levels 1 and 2 the percentage of failures is always 0. However, we can make more demanding checks, which are summarized below[5]:

- Compare the error bars of solutions obtained in the same grid set with first and third-order convection in the turbulence models using 1, 2 or 3 levels.
- Compare the error bars of solutions obtained in different grid sets with the same discretization using 1, 2 or 3 levels.
- Compare the error bars from all the solutions using 1, 2, or 3 levels.

[5]In this case, we have restricted ourselves to the Spalart & Allmaras and BSL $k-\omega$ models

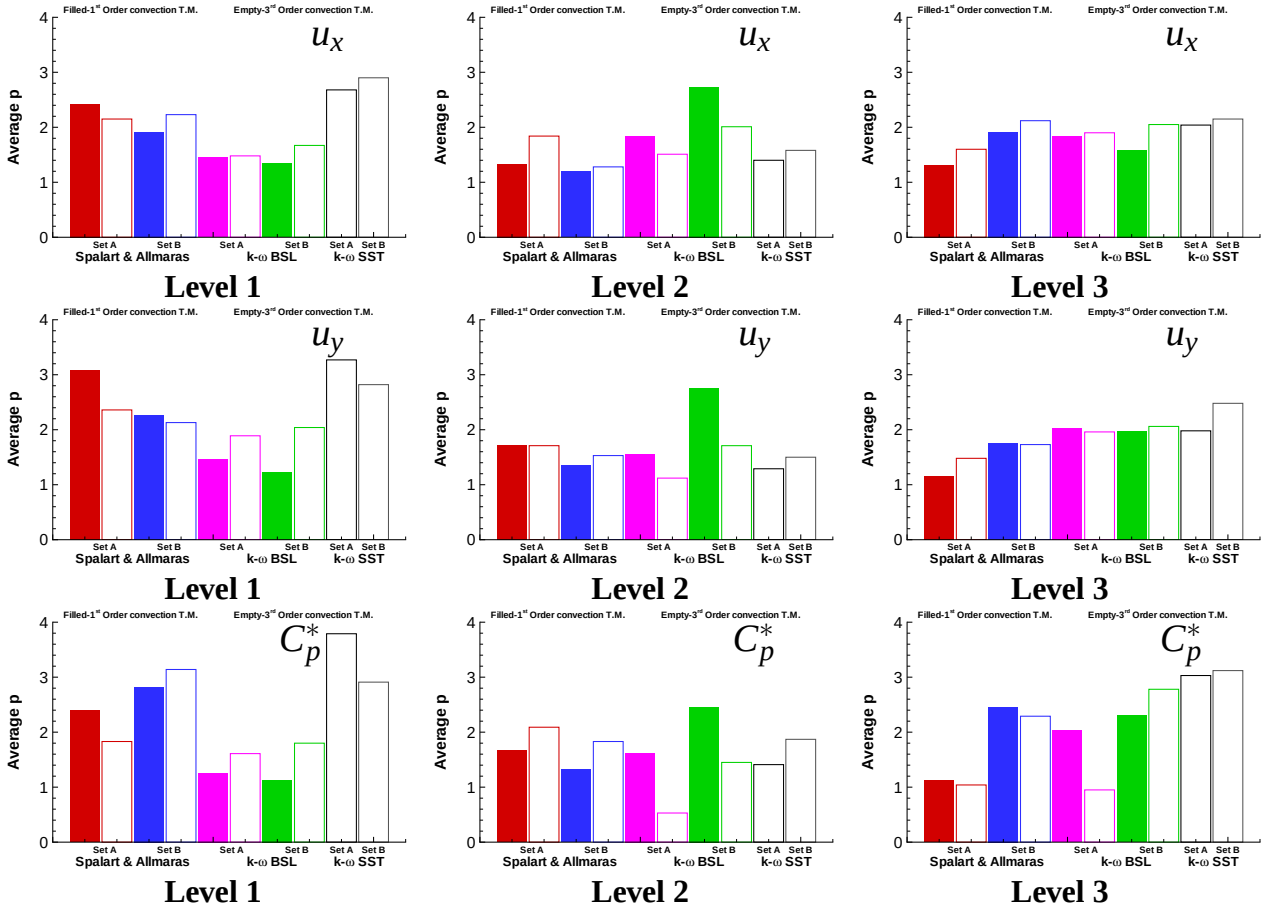

Figure 4: Mean apparent order of convergence at the locations with monotonic convergence. Calculation of the flow over a backward facing step.

Table 1 presents the number of inconsistent error bars for the mean flow variables. In most cases, the percentage of failures is clearly above the 5% target. Interesting features in the data are:

- As expected, the percentage of mismatches between the error bars increases with the grid coarsening.
- The turbulence model has a significant influence on the outcome of the exercise:
  - The Spalart & Allmaras model leads systematically to a higher percentage of inconsistent error bars than the BSL $k-\omega$ model. We recall that the BSL $k-\omega$ results exhibit significant percentages of grid nodes with $p < 0.5$, whereas the Spalart & Allmaras model leads to values of $p > 2.05$.
  - For the finest grid level, the performance of the proposed procedure is close to acceptable (only u_x exhibits 6% of inconsistent error bars for the finest grid solution).
- The comparison between solutions in the same grid set with different discretizations of the convective terms of the turbulence quantities transport equations shows significantly higher percentages of failures than the comparison of error bars for different grids and the same discretization.

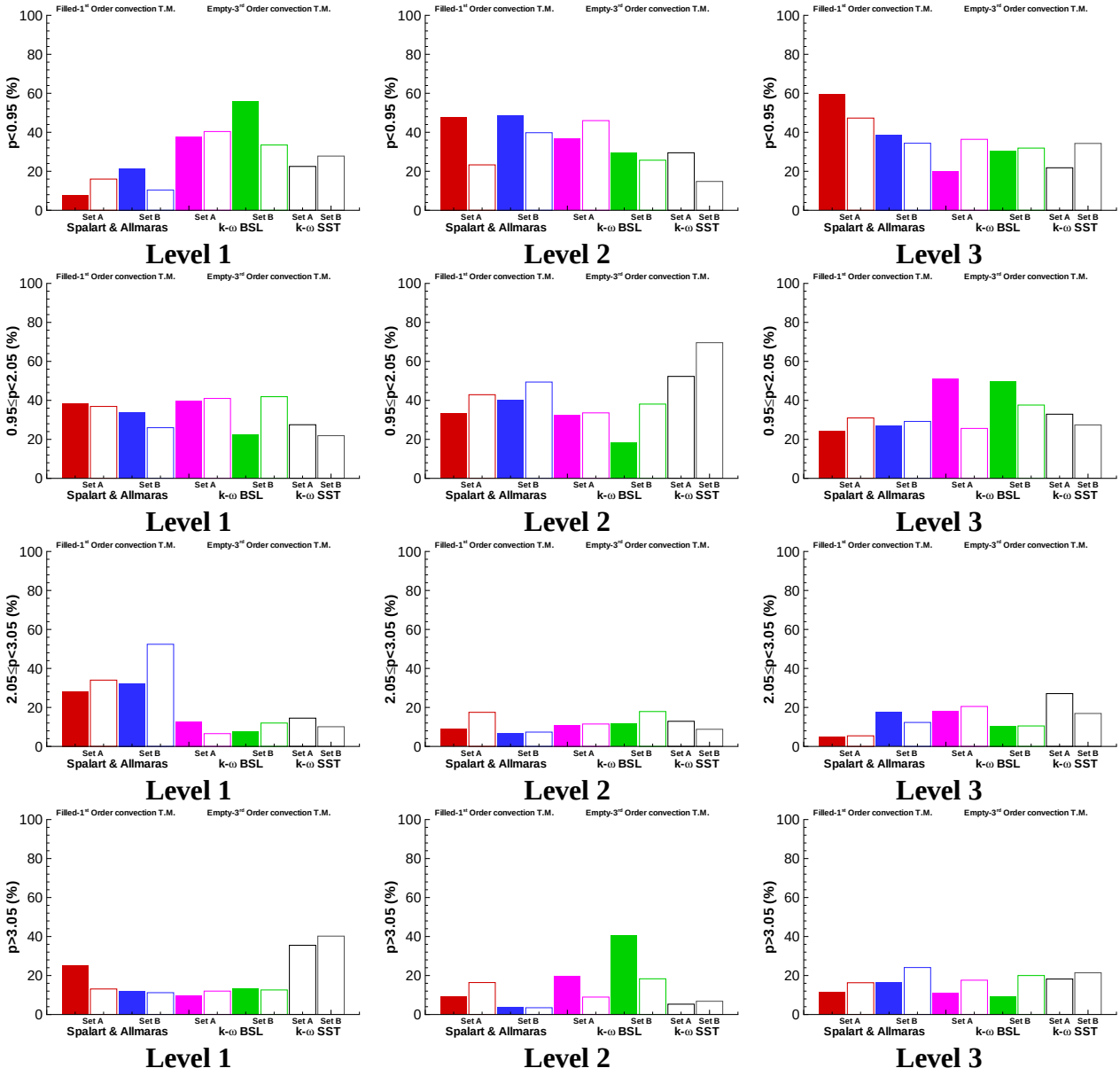

Figure 5: Distribution of the apparent order of convergence at the locations with monotonic convergence. Horizontal velocity component, u_x. Calculation of the flow over a backward facing step.

- In most cases, the percentage of "failures" is higher for the first-order discretization of convection in the turbulence models than for third-order approximations. In fact, excluding all the first-order convection solutions, the performance of the uncertainty estimation method is only poor when the coarsest grids are included. Therefore, the effect of the discretization of the convective terms of the turbulence quantities transport equation on the convergence properties of the mean flow quantities is not negligible.

The results of table 1 show that the present procedure is too optimistic for data referring to coarse grids and first-order convection in the turbulence models. In order to get an idea of how much we should have to increase the safety factors to satisfy the desired goal of 95% confidence [17], we have

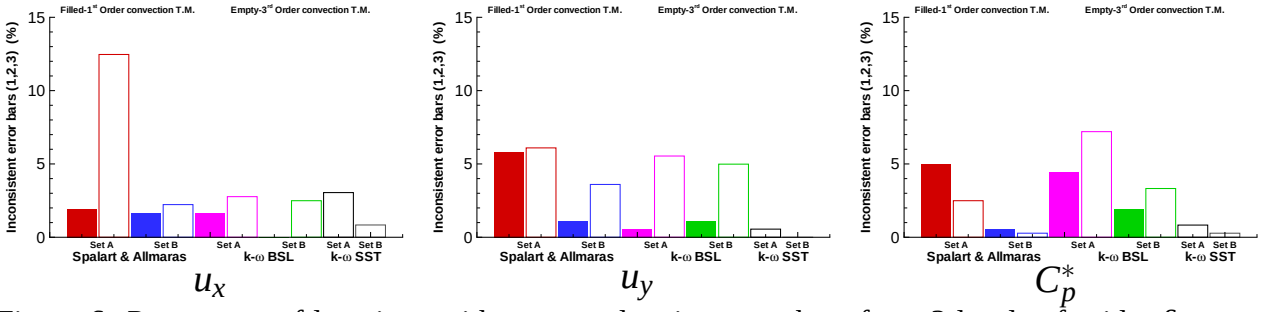

Figure 6: Percentage of locations with non-overlapping error bars from 3 levels of grid refinement. Calculation of the flow over a backward facing step.

Grid Sets	Conv. TM Disc.	Levels	Spalart & Allmaras			BSL $k-\omega$		
			u_x	u_y	C_p^*	u_x	u_y	C_p^*
A	1st	1	14.4	17.8	3.0	1.2	0.5	0.0
	+	1,2	19.1	30.1	21.9	5.9	5.6	6.0
	3rd	1,2,3	36.3	42.2	29.9	11.3	13.3	15.1
B	1st	1	7.2	17.8	38.0	4.0	2.4	3.2
	+	1,2	13.6	24.9	46.4	24.7	19.8	18.9
	3rd	1,2,3	17.8	32.1	48.4	42.5	45.5	43.6
A		1	0.4	1.7	0.0	1.2	1.9	0.0
+	1st	1,2	1.8	7.5	6.6	3.7	5.9	2.6
B		1,2,3	8.1	21.8	13.6	18.3	26.7	22.8
A		1	0.4	0.0	0.3	0.0	0.0	0.0
+	3rd	1,2	3.0	6.7	2.8	0.6	1.0	0.0
B		1,2,3	21.5	21.7	7.4	8.0	14.9	13.5
A	1st	1	26.9	37.1	46.5	6.0	4.5	4.4
+	+	1,2	33.1	47.6	56.1	33.8	27.6	22.5
B	3rd	1,2,3	49.8	54.1	60.3	59.0	56.8	62.6

Table 1: Percentage of locations with non-overlapping error bars from different grid refinement studies and grid densities. Calculation of the flow over a backward facing step.

repeated the same exercise multiplying the estimated uncertainties by 2.4. This would correspond to a factor of safety 3 in the G.C.I, which is recommended by Roache for data outside the asymptotic range [1]. The results are presented in table 2.

The outcome of the exercise is substantially better than in table 1. With these increased safety factors, the method almost satisfies the 95 % confidence criterion. The exceptions are the first-order convection solutions for the Spalart & Allmaras model, where the “standard” safety factors would have to be multiplied by more than 10 to obtain percentages of failures below 5% for the three mean flow variables with all the grid levels tested.

In this type of flow calculations, with a single evaluation of the observed order of accuracy (even in the least square sense) it is practically impossible to decide where data enter the asymptotic range. So our conclusion is that for the backward-facing step flow at hand, and more general for most engineer-

Grid Sets	Conv. TM Disc.	Levels	Spalart & Allmaras			BSL $k-\omega$		
			u_x	u_y	C_p^*	u_x	u_y	C_p^*
A	1st	1	0.9	0.5	0.0	0.0	0.0	0.0
	+	1,2	2.8	7.7	0.0	0.3	1.8	1.4
	3rd	1,2,3	4.3	10.8	2.2	0.6	2.7	1.7
B	1st	1	0.9	1.9	3.9	4.0	0.0	0.0
	+	1,2	1.2	3.9	6.1	0.9	0.0	0.0
	3rd	1,2,3	1.2	5.4	6.4	1.2	0.4	1.7
A		1	0.0	0.0	0.0	0.0	0.0	0.0
+	1st	1,2	0.3	2.5	0.0	0.0	0.9	0.0
B		1,2,3	0.9	3.6	0.3	0.6	1.3	1.4
A		1	0.0	0.0	0.0	0.0	0.0	0.0
+	3rd	1,2	0.3	0.5	0.0	0.0	0.4	0.0
B		1,2,3	1.2	2.0	0.0	0.0	0.9	0.8
A	1st	1	3.8	8.2	18.6	0.3	0.0	0.0
+	+	1,2	6.6	20.1	19.7	2.3	2.8	1.4
B	3rd	1,2,3	9.5	24.7	23.0	3.9	5.6	4.7

Table 2: Percentage of locations with non-overlapping error bars from different grid refinement studies and grid densities, multiplying the estimated uncertainties by 2.4. Calculation of the flow over a backward facing step.

ing computations of turbulent flows, it is necessary to assume the data to be outside the asymptotic range and to apply a safety factor of 3.

4.5 Friction resistance of the top wall

The convergence of the total friction resistance of the top wall with the grid refinement is illustrated in figure 7. The two plots include the results obtained with the Spalart & Allmaras model (finite-difference and finite-volume versions) and with the BSL and SST $k-\omega$ models. Although the grid density of the sets A and B is not identical to the set FV, h_i is computed from the number of nodes in the vertical direction, which is the same for all the finest grids. The plots also include data fits, derived by using the 11 finest grids of sets A and B and 9 finest grids of set FV. The error bars from the three levels of grid refinement presented in the previous section are also included in the plots. For the FV solution, there are only two error bars: for $h_i = h_1$ estimated from the 9 finest grids data and for $h_i = 2h_1$ estimated from the 6 coarsest grids data. The same conditions apply also to the remaining figures presented in this section.

The results of all the solutions per turbulence model are perfectly consistent and it would seem that the finest grid solutions are in the asymptotic range. However, the observed order of accuracy is not always equal to 2.

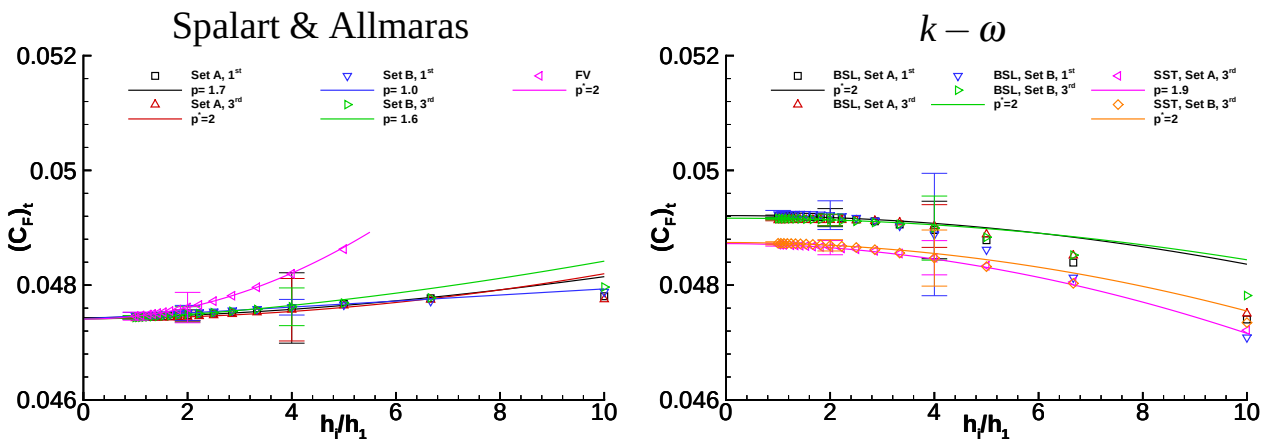

Figure 7: Friction resistance of the top wall as a function of the grid refinement level. Calculation of the flow over a backward facing step.

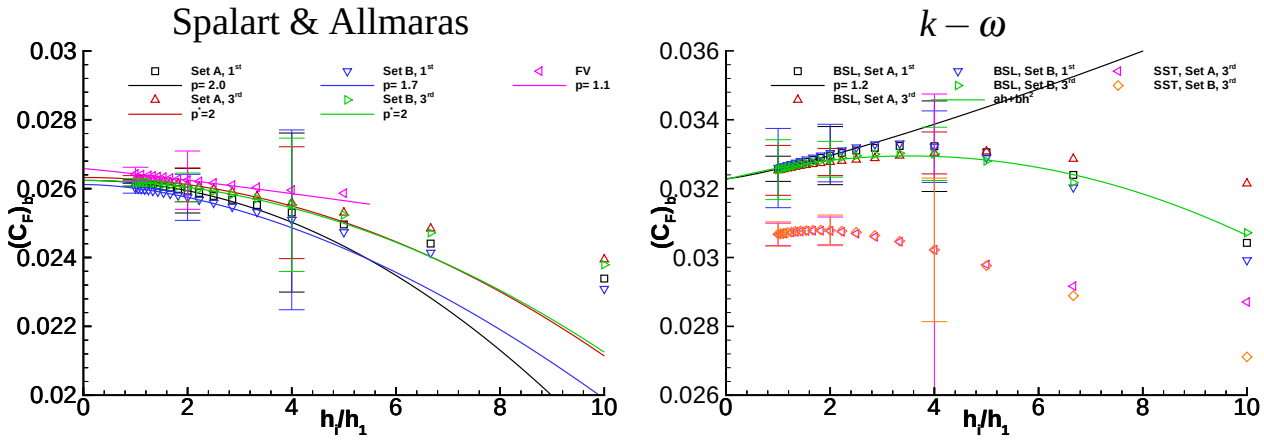

Figure 8: Friction resistance of the bottom wall as a function of the grid refinement level. Calculation of the flow over a backward facing step.

4.6 Friction resistance of the bottom wall

Figure 8 presents the convergence of the friction resistance of the bottom wall with the grid refinement. Because of the flow features, the grid density required to attain the asymptotic range is finer than for the top wall. However, there are more things to be noted:

- In a given grid, the third-order discretization in the convective terms of the turbulence models improves the accuracy of the solution compared to the first-order approach. Furthermore, the deviation from the fits applying to the finest grids starts already for small values of h_i in the first-order case.

- The convergence is not monotonic for the two versions of the $k-\omega$ model, but not oscillating (above and below a mean value). It is a typical example of a case being (wrongly?) classified as "anomalous behaviour". The power series expansion with the first and second order terms is able to make an excellent fit to the data. On the other hand, the fit made for the 11 finest grids

of the SST data indicates apparent divergence, because the maximum of C_F is between $h_i = h_1$ and $h_i = h_2$. In this case, assuming that we have an "anomalous behaviour" condition is the correct choice.

4.7 Pressure resistance of the bottom wall

Figure 9 presents the convergence of the pressure resistance of the bottom wall with the grid refinement. The results suggest the following remarks:

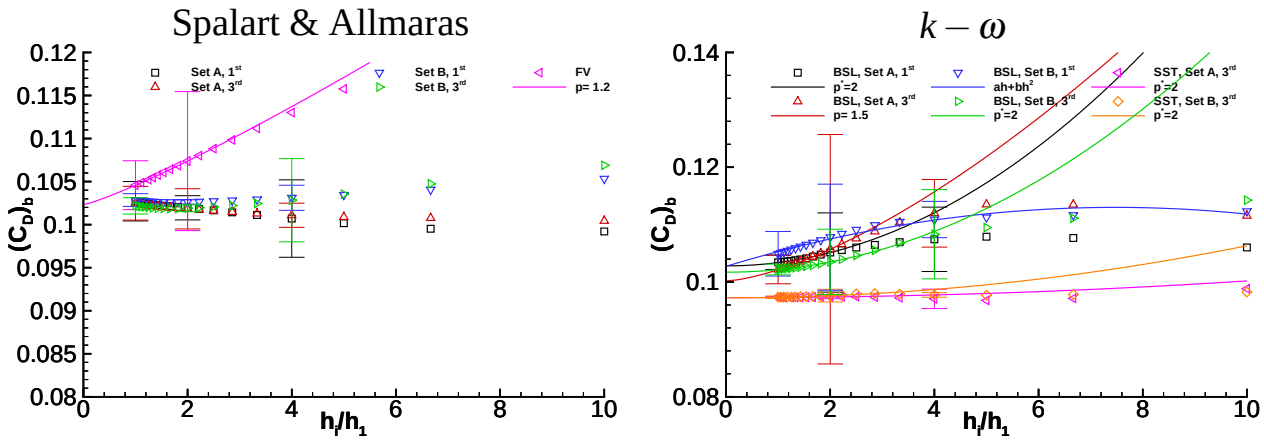

Figure 9: Pressure resistance of the bottom wall as a function of the grid refinement level. Calculation of the flow over a backward facing step.

- Although the different numerical solutions are perfectly consistent for each turbulence model, the convergence properties of C_D are clearly dependent on the selected turbulence model.
  - For the Spalart & Allmaras model, p was not established for the finite-difference results and it is 1.2 for the finite-volume solution. The stronger grid dependency observed in the finite-volume solution is probably originated by the fact that sets A and B always include a node at the corners of the step, which is not guaranteed in set FV. In the finite-difference solutions, the grid topology seems to be more important for the grid dependency than the approximation of the convective terms of the $\tilde{\nu}$ transport equation.
  - In the $k-\omega$ models, there is more influence of the order of approximation of convection for k and ω than for $\tilde{\nu}$. However, in set A the third-order solution in the coarsest grids is less accurate than the first-order predictions. This effect is related to the behaviour of ν_t at the corner of the step, as we will illustrate below.

Figure 9 includes an inconsistent estimation of the error bar for the third-order solution in set A with the BSL $k-\omega$ model. In this case, $U(C_D)$ is equal to 3 times the data range for grids with $h_i \geq 4$. However, without the knowledge of the data from the other grids the estimated error bar would certainly be considered too conservative!

4.8 Re-attachment point

The convergence of the re-attachment point on the bottom wall is illustrated in figure 10. The results are surprising, to say the least.

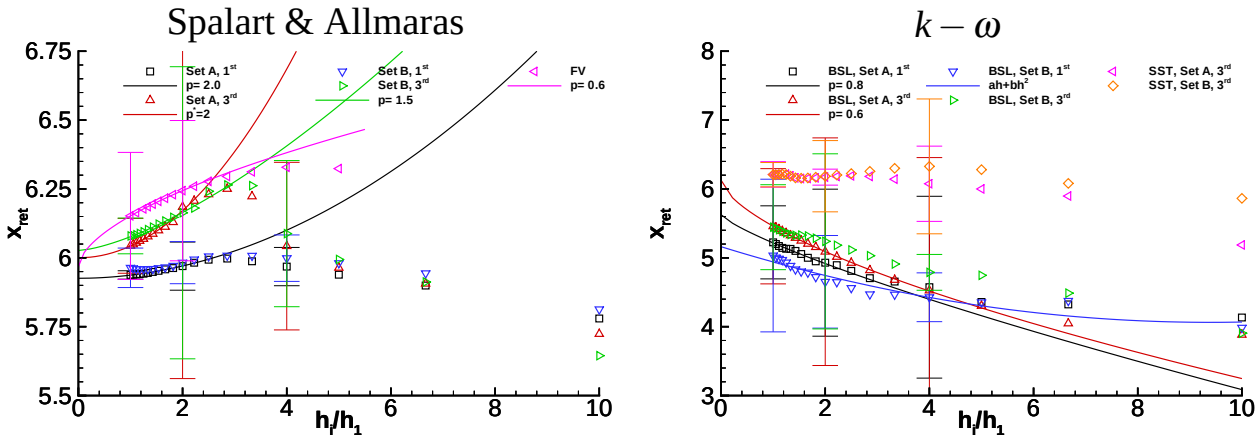

Figure 10: Re-attachment point on the bottom wall as a function of the grid refinement level. Calculation of the flow over a backward facing step.

- None of the convergence histories with the Spalart & Allmaras model is monotonic.
- In both turbulence models, there is a significant effect of the discretization of the convective terms of the turbulence quantities transport equations. As expected, with the finite-difference version, the first-order solutions are less accurate than the third-order predictions, which are closest to the FV solution (also third-order for convection of $\tilde{\nu}$) for the Spalart & Allmaras model.
- If only the two first-order calculations had been performed with the Spalart & Allmaras model, it would have been hard to recognize that the solution is still far from convergence, in particular for set A. Inevitably, the estimated error bar for this case is not conservative.
- A limit applied to the eddy-viscosity determination (main difference between the BSL and SST $k-\omega$ models) is sufficient to change drastically the convergence properties observed for the re-attachment point.

4.9 Horizontal velocity component

Figure 11 presents the convergence with grid refinement of the horizontal velocity component, u_x, at three selected locations: $x = 0, y = 1.1H$, $x = H, y = 0.1H$ and $x = 4H, y = 0.1H$. As expected, the convergence properties are dependent on the selected location, turbulence model, discretization adopted and grid set. The main observations suggested by the data are:

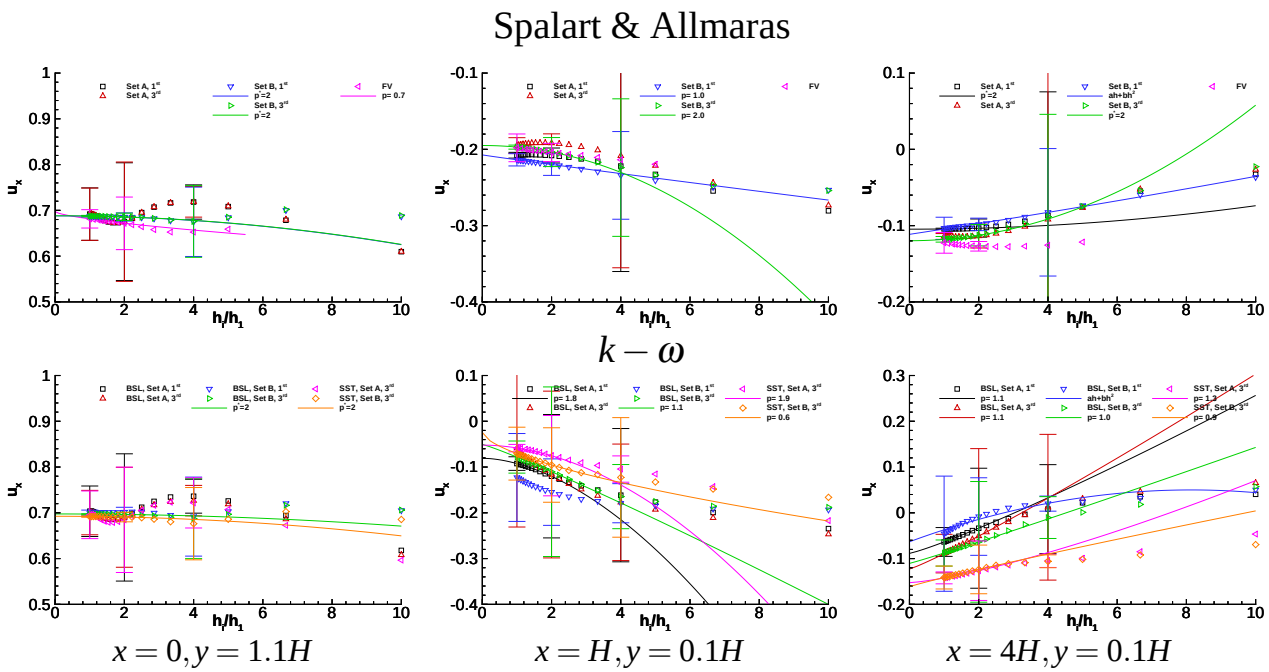

Figure 11: Convergence of u_x as a function of the grid refinement ratio at $x = 0, y = 1.1H$, $x = H, y = 0.1H$ and $x = 4H, y = 0.1H$. Flow over a backward facing step.

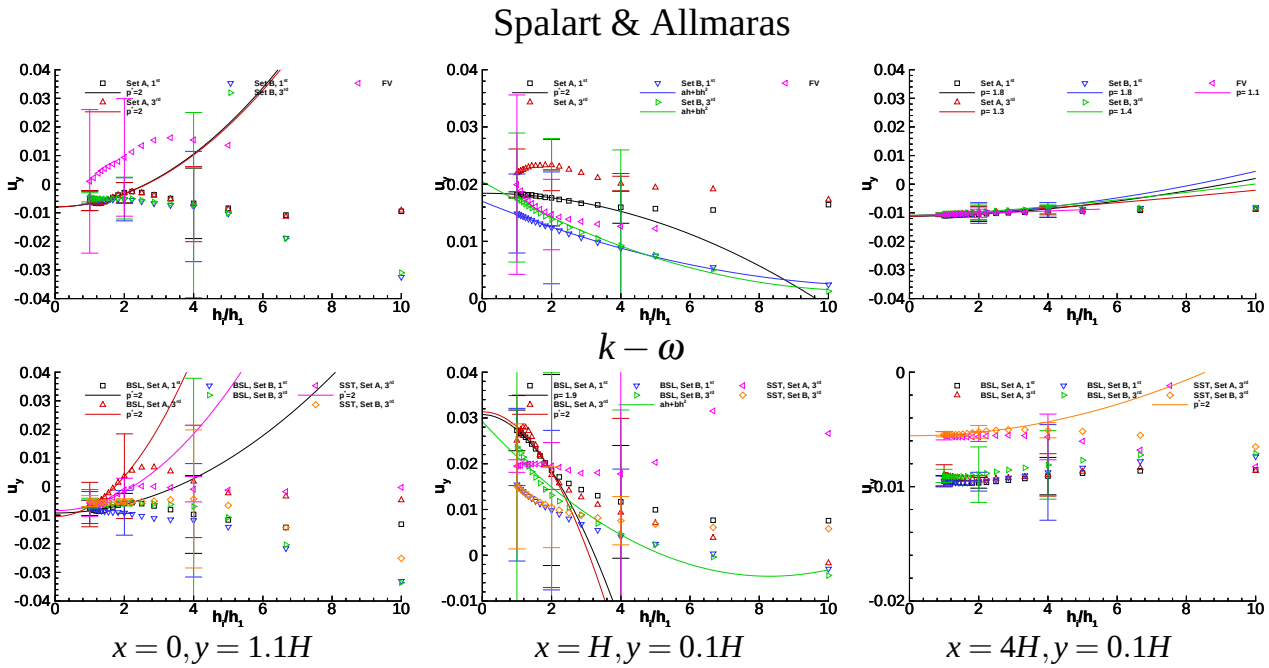

Figure 12: Convergence of u_y as a function of the grid refinement ratio at $x = 0, y = 1.1H$, $x = H, y = 0.1H$ and $x = 4H, y = 0.1H$. Flow over a backward facing step.

- In many cases, it is hard to establish the observed order of accuracy. Nevertheless, it is not difficult to see that most of the grids with $h_i > 2h_1$ are outside the asymptotic range, i.e. almost all the grids used in [8].

- Although the convergence properties are not always identical, the three solutions with third-order convection of $\tilde{\nu}$, A, B and FV, are in excellent agreement.

- With the exception of the location close to the corner of the step, $x = 0, y = 1.1H$, there is a clear improvement in the solution accuracy for the third-order discretizations of the convective terms of the turbulence quantities transport equations.

4.10 Vertical velocity component

Figure 12 shows the convergence with grid refinement of the vertical velocity component, u_y, at three selected locations: $x = 0, y = 1.1H$, $x = H, y = 0.1H$ and $x = 4H, y = 0.1H$. The tendencies observed in the vertical velocity confirm most of the difficulties discussed above for u_x. However, the convergence properties are clearly different from those obtained for u_x. For example, the convergence of u_y at $x = H, y = 0.1H$ and $x = 4H, y = 0.1H$ is astonishingly different. The third-order data obtained in set A at $x = H, y = 0.1H$ with the BSL model is a good example of how difficult it is to make reliable uncertainty estimates for these complex turbulent flows.

4.11 Pressure coefficient

Figure 13 presents the convergence with grid refinement of the pressure coefficient, C_p, at three selected locations: $x = 0, y = 1.1H$, $x = H, y = 0.1H$ and $x = 4H, y = 0.1H$. The convergence properties of C_p are not identical to those observed for the Cartesian velocity components. Nonetheless, most of the remarks made above for the two Cartesian velocity components apply also to the convergence of the pressure coefficient.

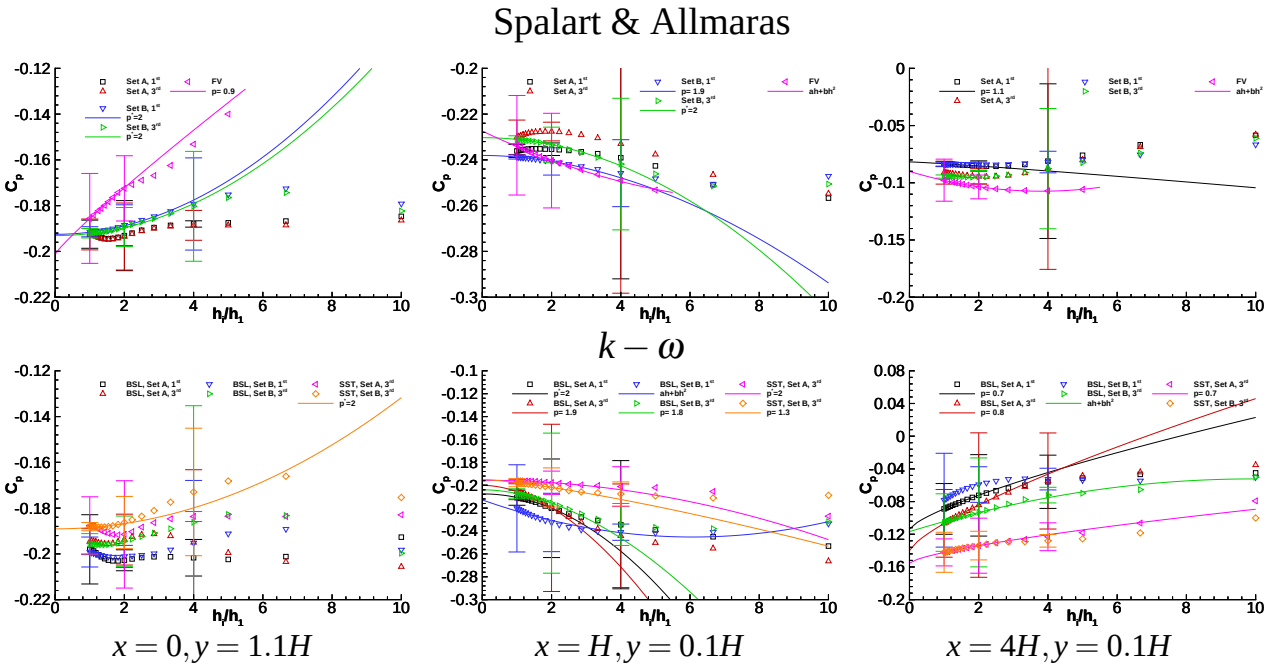

Figure 13: Convergence of C_p as a function of the grid refinement ratio at $x = 0, y = 1.1H$, $x = H, y = 0.1H$ and $x = 4H, y = 0.1H$. Flow over a backward facing step.

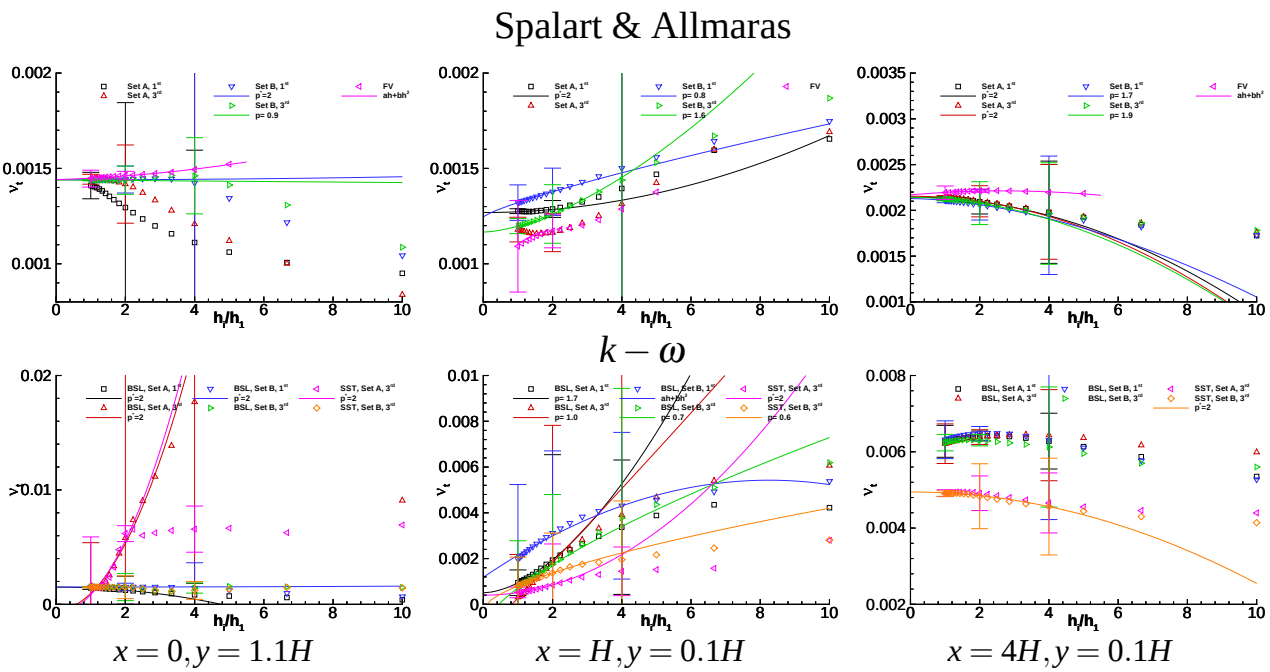

Figure 14: Convergence of ν_t as a function of the grid refinement ratio at $x = 0, y = 1.1H$, $x = H, y = 0.1H$ and $x = 4H, y = 0.1H$. Flow over a backward facing step.

4.12 Eddy-viscosity

Figure 14 presents the convergence with grid refinement of the eddy-viscosity, ν_t, at three selected locations: $x = 0, y = 1.1H$, $x = H, y = 0.1H$ and $x = 4H, y = 0.1H$. We observe the following:

- As expected, the discretization of the convective terms of the turbulence quantities transport equations has a larger influence in ν_t than on the mean flow quantities.
  - For the Spalart & Allmaras model, there is a systematic improvement of the accuracy of the ν_t predictions with the change from first to third-order discretizations.
  - This improvement is not so clear in the BSL solutions. In fact, the troublesome convergence of the mean flow quantities at $x = 0, y = 1.1H$ for the third-order solution in set A is caused by a severe overshoot of the eddy-viscosity that starts for $h_i > 1.4h_1$. The same effect is observed for the SST model, but with a lowest intensity. These overshoots are probably removed with the use of flux limiters.

5 Validation

The Validation Procedure proposed for the 3rd Workshop on CFD Uncertainty Analysis [15] compares two quantities:

- The validation uncertainty, U_{val}.

$$U_{val} = \sqrt{U_{num}^2 + U_{input}^2 + U_D^2}$$

- The validation comparison error, E

$$E = S - D$$

U_{num} is the numerical uncertainty, U_{input} is the parameter uncertainty, U_D is the experimental uncertainty, S is the numerical prediction and D the experimental value. In this exercise we have used the strong model concept [15], i.e. $U_{input} = 0$.

The exercise is performed for the solutions obtained with third-order convection in the turbulence quantities transport equation in the finest grids of set B. U_{num} is estimated with the procedure presented above using the data of the 11 finest grids. The experimental data and their uncertainty are taken from [20, 21]. The procedure identifies deficiencies in the modelling when $|E| > U_{val}$.

5.1 Pressure coefficient along the bottom wall

Figure 15 presents the pressure coefficient along the bottom wall. It contains plots with the usual comparisons between predictions and experiments, although including the not so usual error bars, and the comparison between $|E|$ and U_{val}. This type of representations will also be used in the remainder of this section.

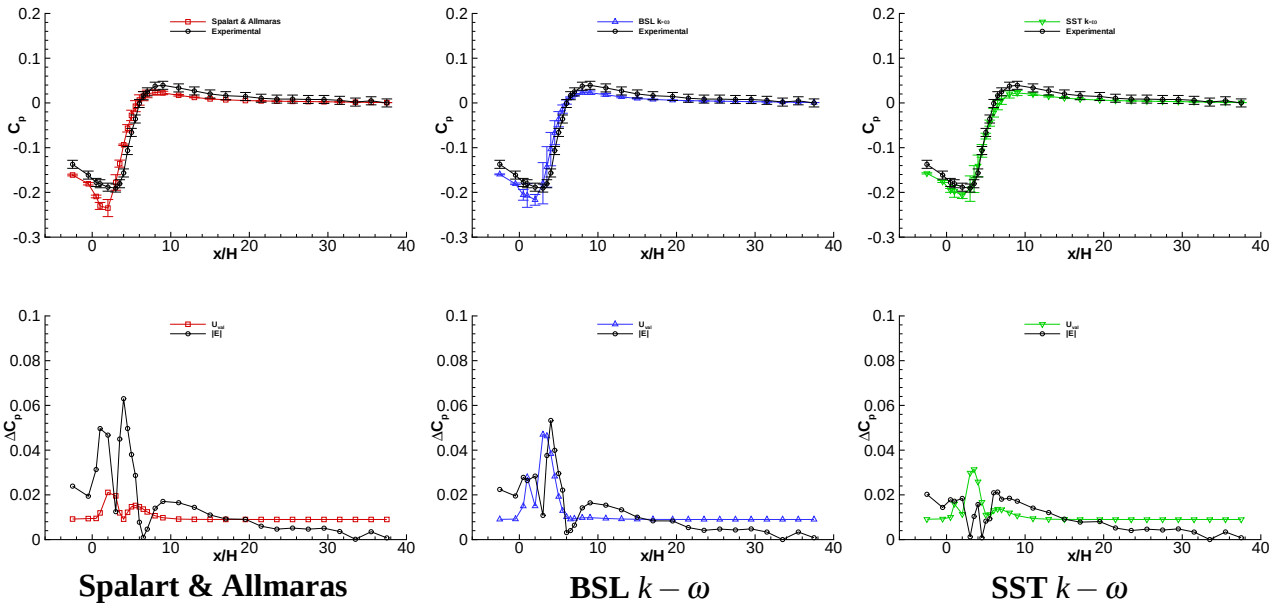

Spalart & Allmaras **BSL $k-\omega$** **SST $k-\omega$**

Figure 15: Validation exercise for the pressure coefficient along the bottom wall. Flow over a backward facing step.

In this case, the main advantage of the classical comparisons is to show where are the highest values of U_{val}. It is clear that downstream of the flow circulation region $U_{val} \simeq U_D$. The comparisons of E and U_{val} indicate that the smallest modelling error is obtained for the SST $k-\omega$ model.

5.2 Pressure coefficient along the top wall

The pressure coefficient along the top wall is depicted in figure 16. In this case, most of the locations exhibit $|E| < U_{val}$ for the three turbulence models and $U_{val} \simeq U_D$. This means that the validation of any improvement in the modelling would require a more accurate experiment.

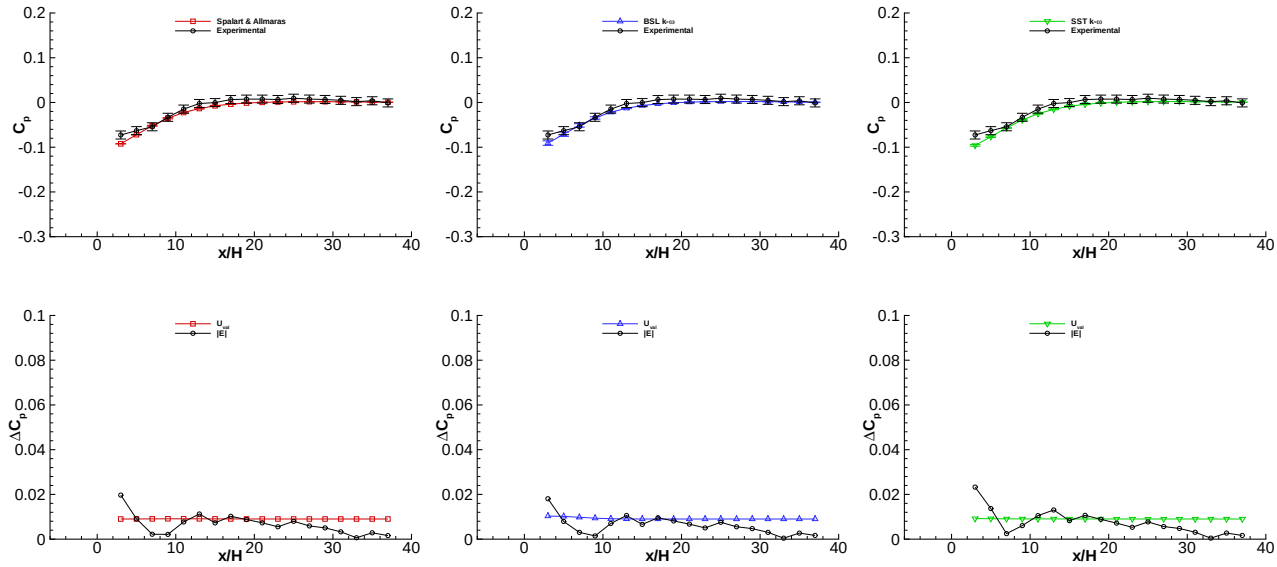

Spalart & Allmaras **BSL $k-\omega$** **SST $k-\omega$**

Figure 16: Validation exercise for the pressure coefficient along the top wall. Flow over a backward facing step.

5.3 Skin-friction coefficient along the bottom wall

Figure 17 presents the distribution of skin friction coefficient, C_f, along the bottom wall. The last two locations with experimental measurements are too close to the outlet of the computational domain. The predictions show a jump in C_f that must be caused by the approximate boundary conditions at the outlet (the pressure is constant at the outlet). As a consequence, U_{num} is one order of magnitude larger than in the rest of domain.

None of the turbulence models exhibits $|E| < U_{val}$ for most of the bottom wall. As for C_p, the smallest values of E are obtained for the SST $k-\omega$ model, but downstream of re-attachment $|E| > U_{val}$. These results suggest an investigation into the effect of the location of the outlet boundary.

5.4 Horizontal velocity profiles

The horizontal velocity profiles at $x = H$, $x = 4H$ and $x = 6H$ are plotted in figure 18. None of turbulence models leads to $|E| < U_{val}$ for the three selected profiles.

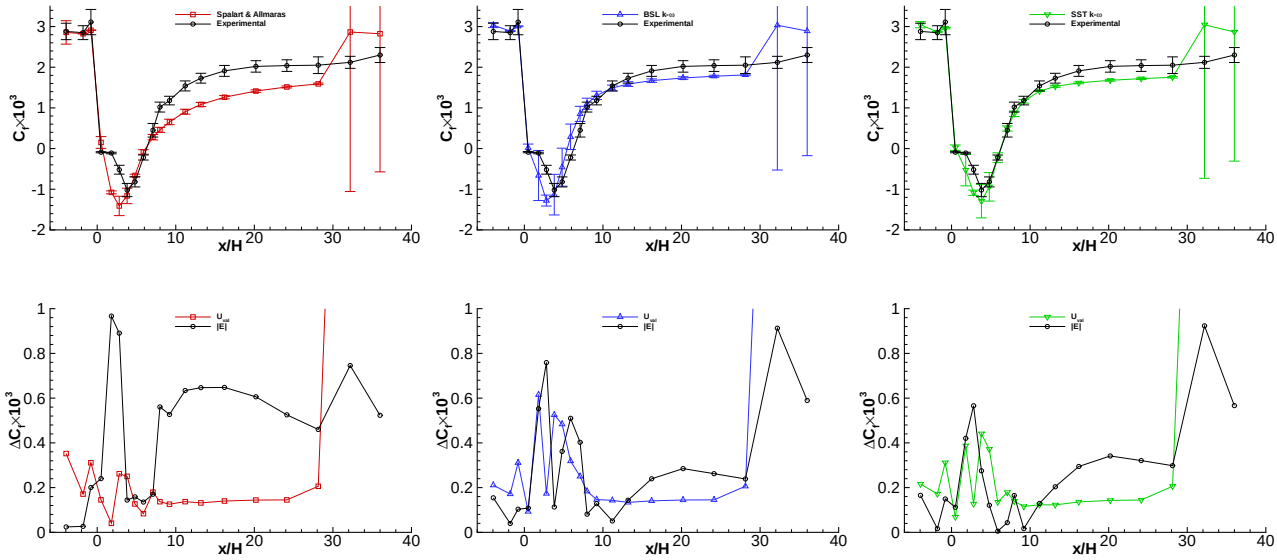

Spalart & Allmaras **BSL $k-\omega$** **SST $k-\omega$**

Figure 17: Validation exercise for the skin-friction coefficient along the bottom wall. Flow over a backward facing step.

At $x = H$ and $x = 4H$ (i.e. in the flow separation region) the BSL and SST models have $|E|$ clearly smaller than the Spalart & Allmaras model. Surprisingly, the smallest values of $|E|$ close to the bottom wall at $x = 6H$ are obtained for the Spalart & Allmaras model and the largest for the SST model. This is puzzling because it is in contradiction with what was observed for the skin friction coefficient. But it is good to bear in mind that the experimental uncertainty is assumed to be $U_D = 0.02(u_x)_D$, which means that it leads to smallest values of U_D at regions where it is hardest to measure.

Suspiciously, the three turbulence models fail at the top wall for the three locations. The thickness of the top boundary-layer seems to be larger in the experiments than in the predictions. We recall that the inlet profiles at the top are obtained from the boundary-layer profiles at the bottom [19]. Therefore, assuming $U_{input} = 0$ might be too optimistic.

5.5 Vertical velocity profiles

The vertical velocity profiles at $x = H$, $x = 4H$ and $x = 6H$ are presented in figure 19. Assuming that U_D is realistic, none of the turbulence models leads to $|E| < U_{val}$. At $x = H$, U_{val} close to the bottom is mainly determined by U_{num}, but for the downstream stations this local increase of U_{num} does not appear. In this case, the differences between the three turbulence models are clearly smaller than for the horizontal velocity component.

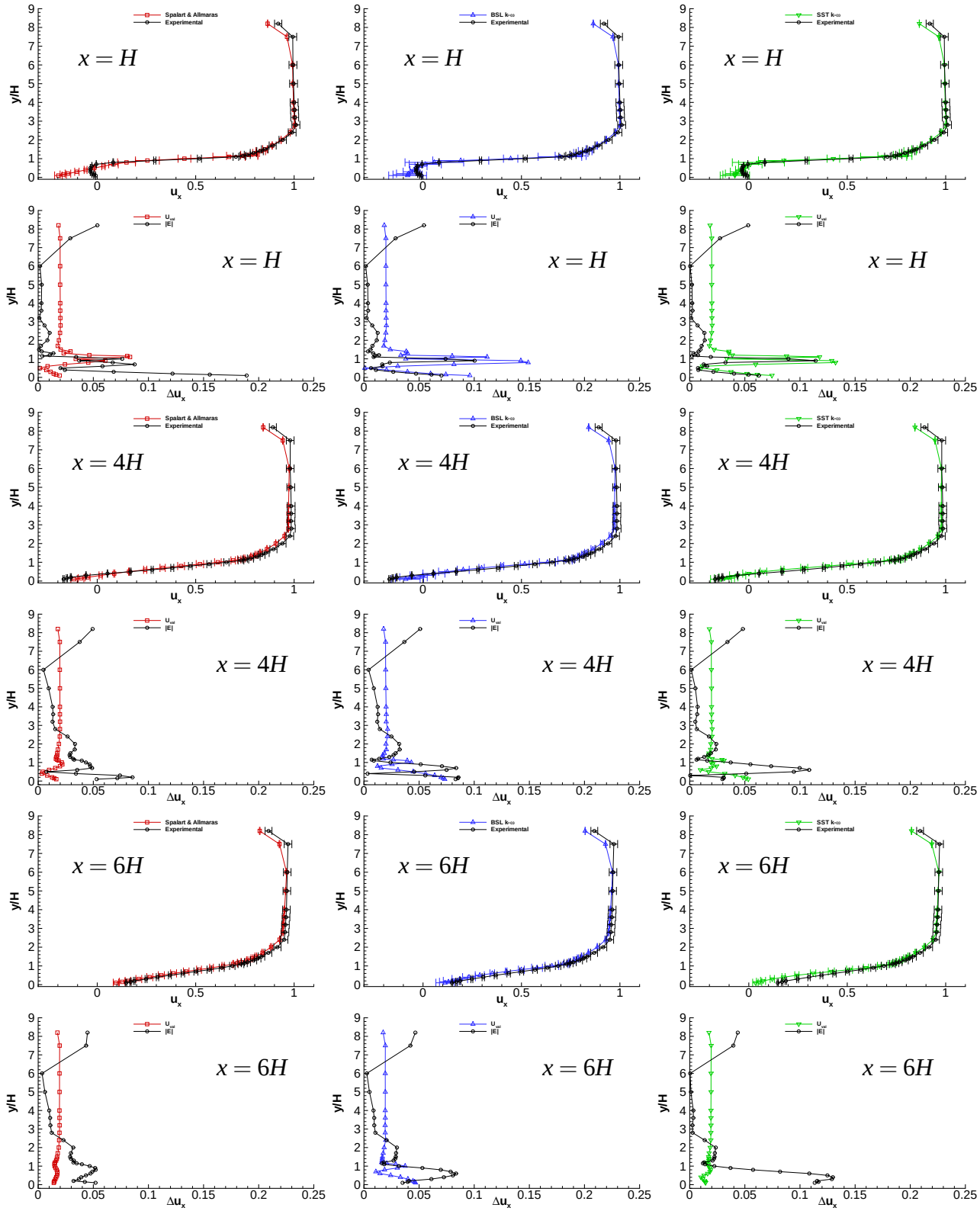

Spalart & Allmaras **BSL $k-\omega$** **SST $k-\omega$**

Figure 18: Validation exercise for the horizontal velocity profiles at $x = H$, $x = 4H$ and $x = 6H$. Flow over a backward facing step.

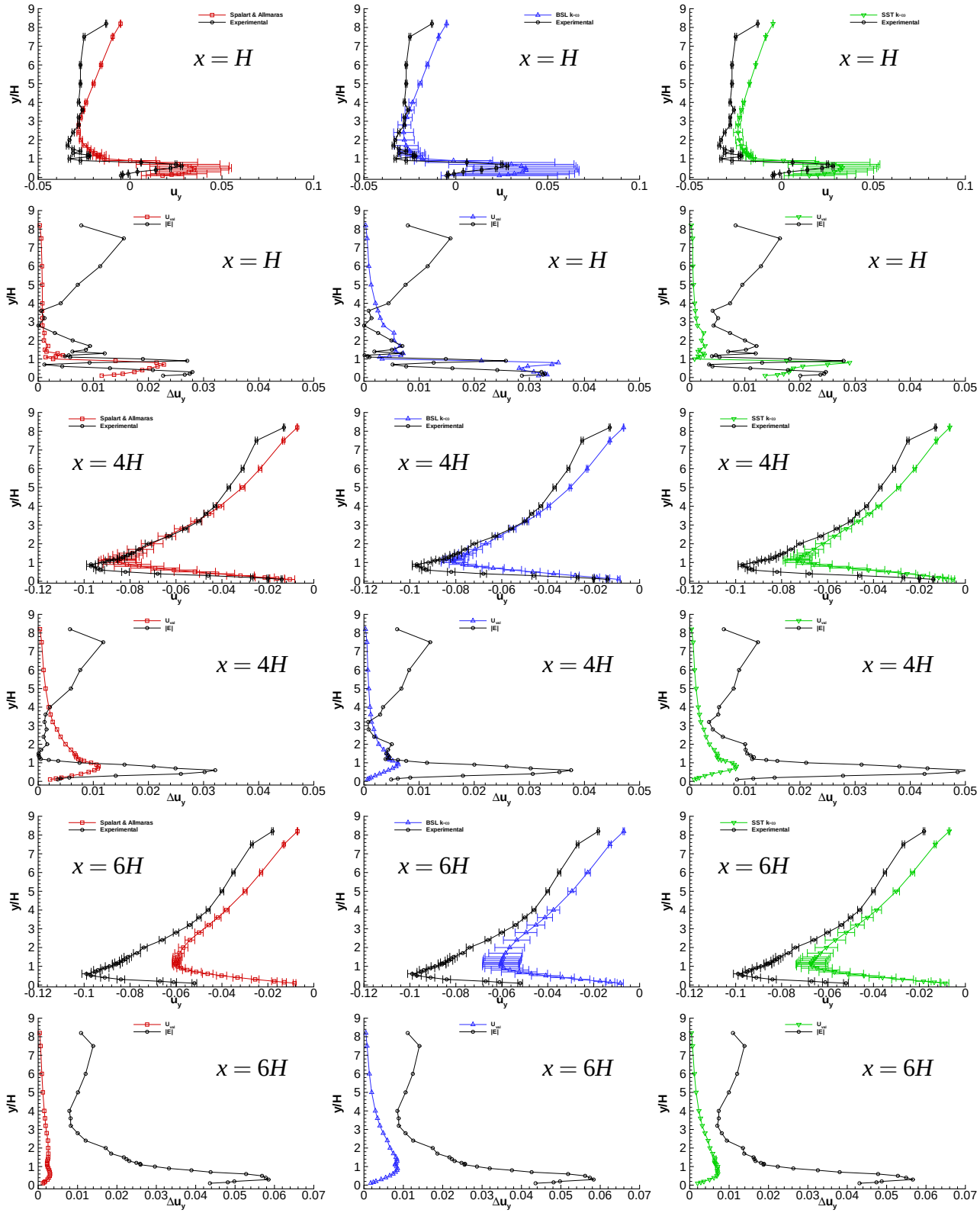

Spalart & Allmaras **BSL $k-\omega$** **SST $k-\omega$**

Figure 19: Validation exercise for the vertical velocity profiles at $x = H$, $x = 4H$ and $x = 6H$. Flow over a backward facing step.

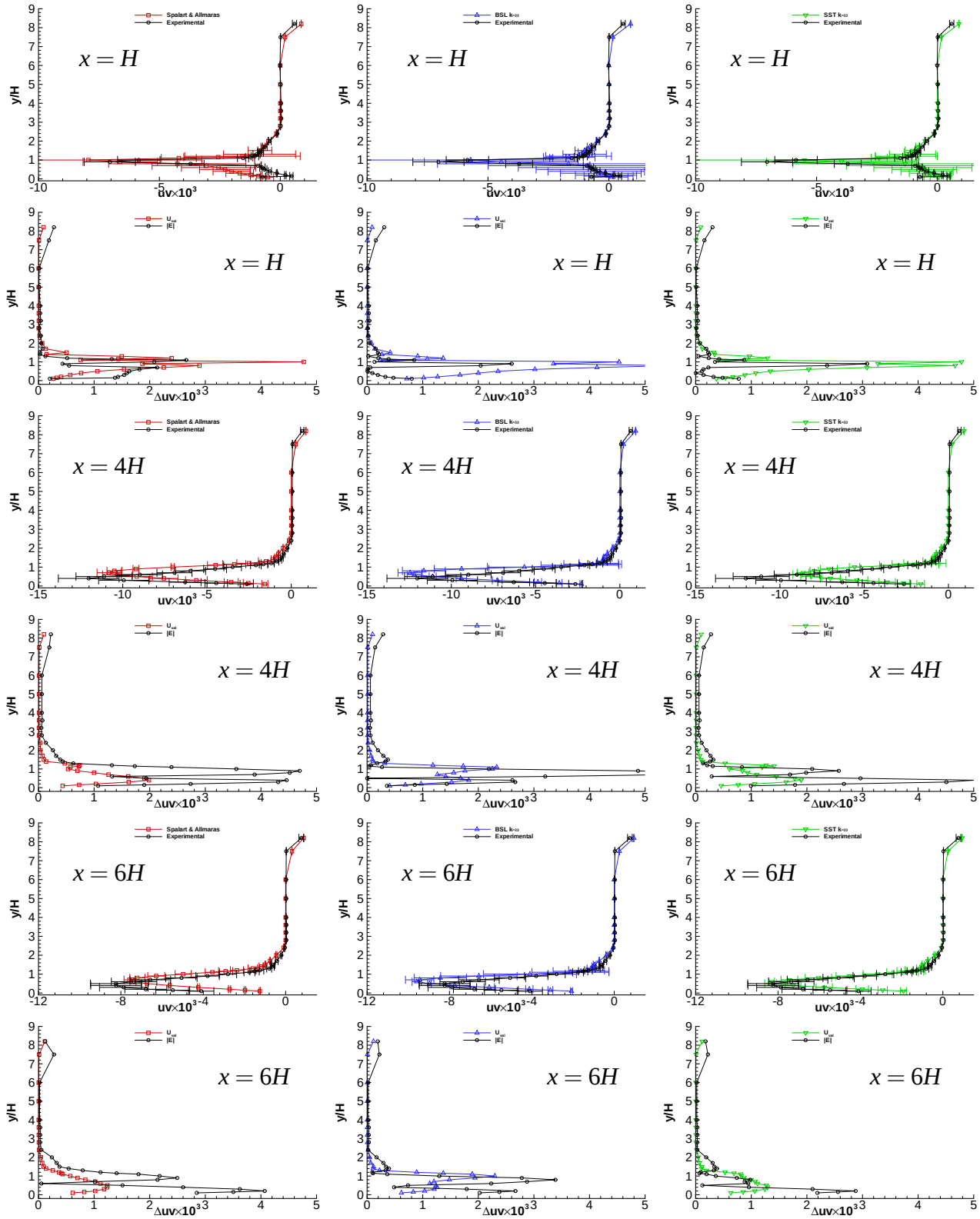

Spalart & Allmaras **BSL $k-\omega$** **SST $k-\omega$**

Figure 20: Validation exercise for the Reynolds-stress profiles at $x = H$, $x = 4H$ and $x = 6H$. Flow over a backward facing step.

Turbulence Model	S	U_{num}	D	U_D	$\|E\|$	U_{val}
Spalart & Allmaras	6.08	0.07	6.26	0.10	0.18	0.12
BSL $k-\omega$	5.44	0.62	6.26	0.10	0.82	0.63
SST $k-\omega$	6.21	0.18	6.26	0.10	0.05	0.61

Table 3: Validation exercise for the re-attachment point. Flow over a backward facing step.

5.6 Reynolds-stress profiles

Figure 20 presents the Reynolds-stress[6] profiles at $x = H$, $x = 4H$ and $x = 6H$. Naturally, there is significant increase of U_{num} close to the bottom wall due to the U_{num} obtained for u_y. This leads to $|E| < U_{val}$ for the three turbulence models, but U_{val} is so high that it would be hard to have $|E| > U_{val}$.

As for several of the previous flow quantities, the smallest values of $|E|$ are obtained for the SST $k-\omega$ model that with the exception of the flow separation region at $x = 4H$ exhibits a remarkable performance in the estimation of uv.

5.7 Re-attachment point

Finally, table 3 presents the results for the re-attachment point, x_{ret}. It is interesting to observe the influence of the turbulence model. The estimated numerical uncertainty differs one order of magnitude, with the lowest for the Spalart & Allmaras model and the highest for the BSL $k-\omega$. The only turbulence model that leads to $|E| < U_{val}$ is the SST $k-\omega$ model. However, U_{val} is roughly 10% of the predicted value, with roughly 7% coming from the numerical uncertainty.

6 Conclusions

This paper presents the evaluation of a method for the estimation of the discretization uncertainty and the application of a recently proposed Validation procedure in the calculation of the two-dimensional flow of an incompressible fluid over a backward facing step. The procedure to estimate the discretization uncertainty is based on a Least Squares version of the Grid Convergence Index complemented with alternative estimators based on power series with fixed exponents and on the data range.

Solution Verification studies have been performed for three grid sets with the finite-difference and finite-volume versions of PARNASSOS using the one-equation turbulence model of Spalart & Allmaras model and the baseline and shear-stress transport variants of the $k-\omega$ two-equation turbulence models proposed by Menter. With the finite-difference version, the grid refinement studies were performed with first and third-order approximations of the convective terms of the turbulence quantities transport equations.

[6]The plotted quantity is uv, the symmetric of the Reynolds stress divided by ρ.

The selected grid sets cover a wide range of grid densities and include unreasonably coarse grids for such flow but also much finer grids than what is commonly used these days in practical RANS calculations. This enables us to assess the performance of the numerical uncertainty estimation at different levels of grid refinement and to evaluate the reliability of the proposed procedure with data clearly outside the asymptotic range. In order to understand the performance of the proposed method, we have also checked the behaviour of the convergence properties with the grid refinement level. The results obtained suggest the following conclusions.

- The main difficulty of methods based on the estimation of the observed order of accuracy is the classification of the apparent convergence condition.
  - For the same solution (same discretization, grid, turbulence model and location), a certain flow quantity can be in the asymptotic range while other flow quantities may be outside it.
  - Even with the least squares approach used in this study, a single evaluation of the observed order of accuracy for a given data set is not reliable. There are two possible solutions to avoid this deficiency:
    - Accept that the data are outside the asymptotic range and consequently apply an increased safety factor.
    - Perform more than one estimate of the observed order of accuracy. However, this will require at least 5 to 6 grids and an extra criterion to decide when the estimation is reliable or not.
- Including first-order discretizations in the turbulence quantities transport equations has a non-negligible effect on the accuracy of the mean flow quantities predictions. It increases the difficulties for the estimation of the numerical uncertainty, because for some flow quantities a grid that is believed to be extremely fine may in fact be too coarse for an accurate solution with a first-order discretization, leading to the problems discussed above.
- With the safety factor set to 3 (data assumed to be outside the asymptotic range) our procedure for estimation of the numerical uncertainty came close to satisfying the 95 % confidence criterion for the turbulent flow over a backward-facing step for fine and coarse grid levels.
- The initial application of the proposed Validation procedure has demonstrated that it represents a huge improvement compared to the common graphical comparison of numerical predictions and experiments. It is interesting to observe that it points out limitations in the modelling, but also shows deficiencies in the numerical simulations and/or in the experiments.

References

[1] Roache P.J. - *Verification and Validation in Computational Science and Engineering* - Hermosa Publishers, 1998.

[2] Proceedings of the 3 Workshop on CFD Uncertainty Analysis - Eça L, Hoekstra M. Eds., Lisbon, October 2008.

[3] Eça L., Hoekstra M., Hay A., Pelletier D. - *A Manufactured Solution for a Two-Dimensional Steady Wall-Bounded Incompressible Turbulent Flow* - International Journal CFD, Vol. 21, N 3-4; March-May 2007, pp. 175-188.

[4] Eça L., Hoekstra M., Hay A., Pelletier D. - *On the Construction of Manufactured Solutions for One and Two-Equation Eddy-Viscosity Models* -International Journal of Numerical Methods in Fluids, Wiley, Vol. 54, 2007, pp. 119-154.

[5] Eça L. - *Calculation of a Manufactured Solution for a 2-D Steady Incompressible Near-Wall Turbulent Flow with PARNASSOS* - IST Report D72-35, January 2006.

[6] Eça L., Hoekstra M. - *Verification of Turbulence Models with a Manufactured Solution* - European Conference on Computational Fluid Dynamics, ECCOMAS CFD 2006, September 2006, Netherlands.

[7] Eça L., Hoekstra M., Hay A., Pelletier D. - *Verification of RANS solvers with Manufactured Solutions* - Engineering with Computers, Vol. 23, N 4, December 2007, pp. 253-270.

[8] Eça L., Hoekstra M. - *Discretization Uncertainty Estimation based on a Least Squares version of the Grid Convergence Index* - 2nd Workshop on CFD Uncertainty Analysis - Instituto Superior Tcnico, Lisbon, October 2006.

[9] José M.Q.B. Jacob, Eça L. - *2-D Incompressible Steady Flow Calculations with a Fully Coupled Method* - VI Congresso Nacional de Mecnica Aplicada e Computacional, Aveiro, April 2000

[10] Hoekstra M. - *Numerical Simulation of Ship Stern Flows with a Space-marching Navier-Stokes Method* - PhD Thesis, Delft 1999.

[11] Spalart P.R., Allmaras S.R. - *A One-Equations Turbulence Model for Aerodynamic Flows* - AIAA 30th Aerospace Sciences Meeting, Reno, January 1992.

[12] Menter F.R. - *Two-Equation Eddy-Viscosity Turbulence Models for Engineering Applications* - AIAA Journal, Vol.32, August 1994, pp. 1598-1605.

[13] Wilcox D.C. - *Turbulence Modeling for CFD* - DCW Industries, Second Edition, March 2000.

[14] ASME Committee PTC-61, 2008, ANSI Standard V&V 20. ASME Guide on Verification and Validation in Computational Fluid Dynamics and Heat Transfer, (expected) 2008.

[15] *Validation Procedure for 3rd Workshop on CFD Uncertainty Analysis* in Proceedings of the 3 Workshop on CFD Uncertainty Analysis - Eça L, Hoekstra M. Eds., Lisbon, October 2008.

[16] Eça L, Hoekstra M. - *An Evaluation of Verification Procedures for CFD Applications* - 24th Symposium on Naval Hydrodynamics, Fukuoka, Japan, July 2002.

[17] Roache P.J. - *Error Bars for CFD* - AIAA-2003-048, 41th Aerospace Sciences Meeting, Reno NV, January 2003.

[18] Saad Y, Schultz M.H. - *GMRES: a generalized minumum residual algorithm for solving non-symmetric linear systems* - SIAM Jnl. Sci. Statist. Comp., Vol. 7, pp 856-869, 1986.

[19] Proceedings of the Workshop on CFD Uncertainty Analysis - Eça L, Hoekstra M. Eds., Lisbon, October 2004.

[20] David M. Driver, H. Lee Seegmiller - *Features of a Reattaching Turbulent Shear Layer in Divergent Channel Flow* - AIAA Journal, Vol. 23, N 2, February 1985, pp. 163-171.

[21] Srba Jovic, David M. Driver - *Backward-Facing Step Measurements at Low Reynolds Number* - NASA Technical Memorandum 108807, Ames Research Center, February 1994